JOURNAL OF PROPULSION AND POWER
Vol. 17, No. 2, March–April 2001

Structural Dynamic Analysis of Solid Rocket Motor Resonant Burning

K. W. Dotson* and J. M. Womack†
The Aerospace Corporation, Los Angeles, California 90009-2957
and
P. J. Grosserode‡
Orbital Sciences Corporation, Chandler, Arizona 85248

The term resonant burning is used by structural dynamicists to describe the coincidence of vortex shedding inside solid rocket motors with frequencies of longitudinal acoustic modes of the combustion chamber. The corresponding thrust oscillations excite launch vehicles that use solid rocket motors; however, system responses from resonant burning are generally enveloped by those for other flight events, and, traditionally, the design of primary launch and space vehicle structure has not been established by the resonant-burning dynamic environment. Recently, though, this phenomenon has emerged as a major dynamic event for new small-sized launch vehicles with single-segment motors as stages. An overview of resonant burning is provided, with an emphasis on features that influence structural dynamic analyses. Statistical assessments of motor internal pressure oscillations, and of spacecraft loads induced by resonant burning, are conducted. The results indicate that the phenomenon cannot generally be characterized by a normal probability distribution and that care must be taken when defining a resonant-burning environment for structural design. It is also shown that this excitation source is quasi periodic and that structural dynamic analyses that use stationary thrust oscillations can severely overpredict spacecraft accelerations.

Nomenclature

c	=	motor internal speed of sound, ft/s
f	=	frequency, Hz
k	=	empirical normalized vortex convection speed, dimensionless
L	=	length of motor chamber, ft
L_v	=	distance between vortex initiation and impingement points, ft
M	=	Mach number of motor internal flow, dimensionless
m	=	integer number of vortices, dimensionless
n	=	mode number, dimensionless
p	=	oscillatory pressure, psi
Sr	=	Strouhal number, dimensionless
t	=	time after ignition (burning time), s
U	=	mean internal flow velocity, ft/s
α	=	empirical normalized acoustic time lag, dimensionless

Subscripts

a	=	acoustic mode
v	=	vortex shedding

I. Introduction

MANY launch vehicles have solid rocket motors as stages. For example, the Titan IV, the space shuttle, and the Ariane 5 use large multisegment motors, whereas the Delta, Taurus, and Athena use small single-segment motors.[1] A schematic of the Taurus launch vehicle is provided in Fig. 1.

During combustion, the shedding of vortices in the internal flow of solid rocket motors can become organized and lead to self-induced oscillations in the internal pressure.[2] The launch vehicle's longitudinal thrust is primarily defined by time histories of the internal pressure at the motor's head end and aft dome. Hence, vortex-induced thrust oscillations excite the coupled launch vehicle–space vehicle system predominately in the axial direction.

Although the amplitude of the thrust oscillations may account for only a few percent of the overall longitudinal thrust profile, this excitation source can represent a major flight event for the design of motor hardware,[3] avionics equipment,[4] and spacecraft structure.[5] The pressure oscillation frequencies roughly coincide with those of the longitudinal acoustic modes of the solid rocket motor,[2] and the phenomenon is commonly called resonant burning by structural dynamicists. Industry also uses the terms motor buzz and motor sine vibration, whereas propulsion literature favors the rubric combustion instability.

Unstable motor combustion has been studied since the late 1940s[6]; however, there is a paucity of literature on the computation of launch vehicle and spacecraft loads induced by this excitation. The main objective of this paper is to address this need and to provide general considerations for resonant-burning load analyses. It will be shown, for instance, that, although the phenomenon is commonly called resonant, the motor pressure oscillations are quasi periodic, that is, not sinusoidal with a fixed frequency and amplitude. This nonstationary character influences the formulation of an accurate structural dynamic analysis.

The amplitude of the maximum thrust oscillations can vary significantly, even in a set of motors of ostensibly identical construction. Statistical modeling of this flight-to-flight variation can affect the design of the launch vehicle–space vehicle system and has not been adequately investigated. This paper studies the resonant-burning probability distribution using available test and flight data for both large multisegment and small single-segment motors.

II. Resonant-Burning Phenomenon

The motor internal flow during combustion tends to shed vortices at propellant grain discontinuities or at objects protruding into the flow.[7] For example, vortex shedding is known to occur at rubber annular inhibitors,[8] at gaps between motor segments,[9] and at propellant fins.[10]

Received 10 March 1999; revision received 20 June 2000; accepted for publication 1 August 2000.

*Engineering Specialist, Structural Dynamics Department, P.O. Box 92957-M4/909. Senior Member AIAA.
†Director, Statistics and Satellite Replenishment Office, P.O. Box 92957-M4/997.
‡Senior Principal Engineer, Launch Systems Group, 3380 South Price Road.

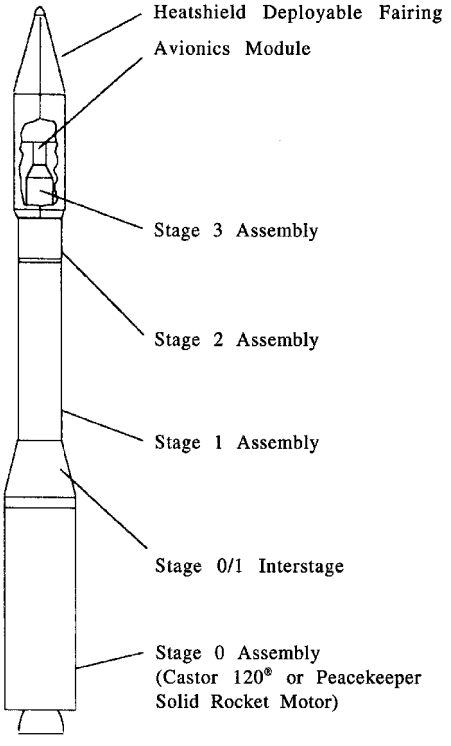

Fig. 1 Taurus launch vehicle.

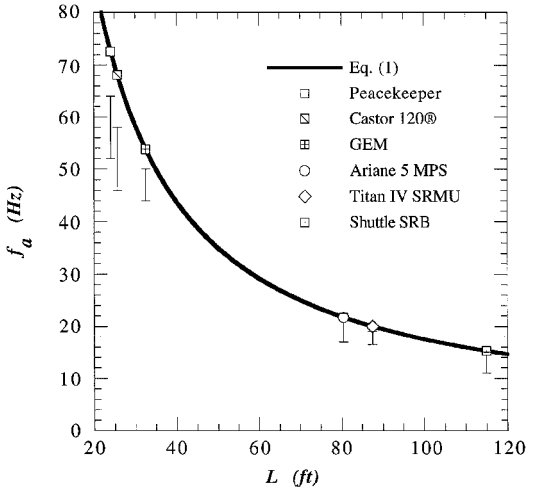

Fig. 2 Motor fundamental acoustic mode frequency: heavy line corresponds to one-dimensional combustion chamber with closed ends and bars indicate ranges observed in static firing data.

A. Motor Acoustic Modes

It was first shown in 1973 that the internal pressure oscillations from resonant burning are caused by coupling of vortex shedding with the acoustic modes of the motor chamber.[11] Because an infinite number of acoustic modes exist, the pressure oscillations may theoretically have many frequency components. However, static firing data for numerous motor designs indicate that the pressure oscillations are dominated by coupling with, at most, the first two acoustic modes.[7,9,10,12,13]

When the motor is modeled as a cavity with closed ends, the frequencies of its longitudinal acoustic modes can be approximated by

$$f_a = nc/2L \tag{1}$$

in which the speed of sound c is taken herein as 3500 ft/s. Equation (1), with $n = 1$, is shown in Fig. 2 for several solid rocket motors.

The Taurus launch vehicle uses either the Peacekeeper or Castor 120® motor as a first stage.[1] The Castor 120 is also used for stages of the Athena (previously known as the Lockheed Launch Vehicle).[1] Graphite-epoxy motors (GEMs) are mounted in a ring at the base of the Delta launch vehicle.[1]

It is shown in the next section that the pressure oscillation frequency varies about the acoustic mode frequency. The bars in Fig. 2 indicate the ranges of the fundamental acoustic mode frequency evident in static firing test data.[9,10,13–16] The lowest and highest values in the range correspond, respectively, to the beginning and end times of resonant burning. The acoustic mode frequency increases with time because burning of the propellant changes the geometry of the combustion chamber. A simple modification to Eq. (1) may be introduced to approximate this secondary effect.[2] The highest value in the range is reasonably close to the estimate from Eq. (1) because the combustion chamber approaches a uniform cavity, albeit with an opening at the nozzle throat.

The coincidence of the longitudinal acoustic mode and vortex shedding frequencies is defined by limit-cycle oscillation of a nonlinear system involving complex interactions between the unsteady flowfield and the combustion processes.[2] Unfortunately, state-of-the-art combustion stability computer codes cannot accurately predict a solid rocket motor's pressure oscillation time history.[17,18] Hence, data recorded during static firing tests or launch vehicle flight are required for resonant-burning load analyses.

B. Vortex Shedding

Although the combustion process is complicated, a simple acoustic feedback model can often be used to explain variations in the pressure oscillation frequency. In the model,[9] the vortex shedding frequency is a function of the mean internal flow velocity such that

$$f_v = Sr(U/L_v) \tag{2}$$

The Strouhal number for m vortices in the distance L_v can be approximated by[9]

$$Sr = (m - \alpha)/(M + 1/k) \tag{3}$$

The empirical constant k defines the normalized vortex convection speed and α defines the normalized lag time between vortex impingement and the generation of an acoustic pulse.[9] For the Titan IV solid rocket motor upgrade (SRMU)[9] and Peacekeeper,[16] $k = 0.57$ and $\alpha = 0.25$ yield an excellent fit with static firing data. The Mach number of solid rocket motor internal flow is small (typically $\ll 0.3$), and the effect of M in Eq. (3) is generally minor.

After the pressure buildup at ignition, the mean internal flow velocity U decreases monotonically. Hence, as the motor burns, Eq. (2) for a fixed value of m initially approaches, then recedes from, the slowly increasing acoustic mode frequency. To remain near the acoustic mode frequency, the integer m increases. For this new value of m, the vortex shedding frequency eventually decouples from that of the acoustic mode, and the integer m increases again. The vortex shedding frequency, therefore, varies about the frequency of the acoustic mode and only equals it at discrete time points. The pressure oscillations are generally largest when $f_v = f_a$ (Ref. 9). Physically, the acoustic feedback model implies that there are an integer number of vortices between the initiation and impingement points and that the number of vortices increases, in discrete jumps, with burning time.

The frequency variation defined by Eq. (2) is plotted in Fig. 3 using the predicted Peacekeeper internal flow velocity during the 4–14 s time period. Fins and webs, cut into the propellant at the aft end of the motor to control burning, represent the only grain discontinuities at which vortex shedding can occur. (Details of the Peacekeeper and Castor 120 geometry are provided in Ref. 10.) The L_v value corresponds to vortex initiation at the forward face of these fins and impingement on the nozzle lip. Frequencies extracted from waterfall plots of spectral density, computed using pressure oscillation measurements from four static firing tests, are included in Fig. 3 for comparison. The agreement between the acoustic feedback

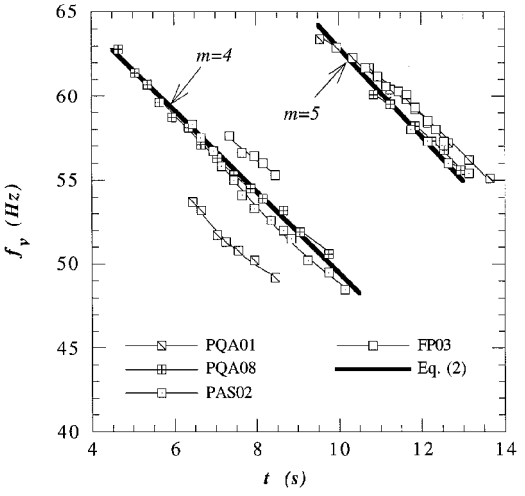

Fig. 3 Comparison of Peacekeeper static firing pressure oscillation frequencies with acoustic feedback model: number of vortices (value of *m*) increases to maintain coupling with the motor's longitudinal acoustic mode.

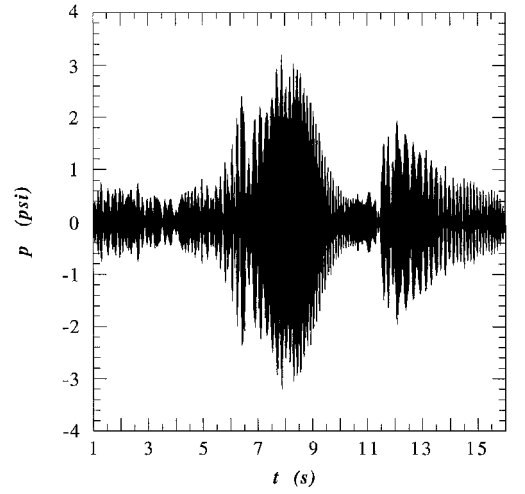

Fig. 4 Peacekeeper PAS02 static firing pressure oscillation history: maximum amplitudes correspond to coincidence of vortex shedding with the motor's fundamental acoustic mode frequency.

model and static firing data is not always as good as that shown, and the model is sometimes more heuristic than predictive.

Pressure oscillations from the Peacekeeper PAS02 static firing test are plotted in Fig. 4 for the 1–16 s time period. The maximum amplitudes occur toward the middle of the two frequency tracks plotted in Fig. 3. It is expected that the frequency of the vortex shedding is coincident with that of the Peacekeeper fundamental acoustic mode at these two time points. Therefore, it appears that the frequency of the longitudinal acoustic mode increased from roughly 53 to 58 Hz during the 8–12 s time period.

The trend shown in Fig. 3 (in which the pressure oscillation frequency decreases with time, then jumps, then decreases, etc.) is evident in static firing test data for numerous solid rocket motors.[7,9,10,13,14] To predict loads accurately, the structural dynamic analysis must account for this nonstationary behavior.

III. System Impact of Resonant Burning

The oscillatory component of the longitudinal thrust excites axial modes and coupled axial–lateral modes of the combined launch vehicle–space vehicle system. It is often stated that the reason for interest in solid rocket motor resonant burning is its effect on loads and, consequently, structural design.[2,3,7] It appears that, in the past, the loads of concern were restricted to motor hardware[3] and system subcomponents.[7]

Table 1 Peacekeeper pressure oscillation (peak-to-peak) amplitude, psi

	Interval, s				
Static firing	1–4	4–7	7–10	10–13	13–16
DM1	0.8	6.7	7.2	1.9	1.7
DM2	1.7	8.3	10.0	2.5	2.3
DM3	1.2	11.2	11.7	3.7	2.0
DM6	1.9	4.3	8.9	4.5	2.4
DM9	2.1	3.5	11.3	3.8	4.1
FP03	3.1	5.6	9.4	11.2	3.3
MQ01	0.8	4.0	3.6	1.6	1.3
PQA01	1.3	9.3	8.5	9.2	2.9
PQA02	2.0	11.0	8.5	1.4	0.8
PQA03	2.1	6.2	6.3	4.5	1.9
PQA04	4.9	5.7	1.6	1.6	0.8
PQA05	4.2	5.5	4.7	2.5	0.9
PQA06	4.9	7.4	4.8	1.4	0.7
PQA07	2.4	5.7	2.7	4.1	1.7
PQA08	1.0	4.7	5.5	4.1	1.3
PAS02	1.5	4.9	6.4	3.9	2.8
Q04A	3.6	11.8	7.9	3.2	1.4

Generally, the critical loads for medium- and heavy-lift launch vehicles and their payload structures are defined by liftoff, atmospheric flight, engine ignitions and shutdowns, and staging and separation events.[19] In other words, even though resonant burning occurs for medium- and heavy-lift vehicles with solid rocket motors as stages, it has not been a flight event that required analysis during design load cycles for primary structure.[19]

For small-sized launch vehicles with solid rocket motors as stages, resonant burning can produce spacecraft loads that exceed those induced by the flight events just listed. There are two prime reasons for this change from the historical trend: 1) The solid rocket motors make up the vehicle core for small-sized launch vehicles, such that the thrust oscillations and the spacecraft interface are collinear (cf. Fig. 1). 2) The solid rocket motors used are relatively short, such that the thrust oscillation frequencies are higher than those for long motors and, consequently, more likely to excite structural modes in the frequency range where other flight events do not dominate. Given the trend in the aerospace industry toward smaller and cheaper launch vehicles, which favor solid rocket motors over liquid propulsion, resonant burning may be emerging as a new critical analysis for design load cycles.

The importance of the resonant-burning phenomenon with respect to two of the more traditional load events is shown in Fig. 5. The absolute shock spectra correspond to predicted c.g. accelerations for a spacecraft that was successfully flown on the Taurus launch vehicle. Results for other load events, such as wind gust and stage burnouts and separations, are not shown because they do not contribute to the spectral envelope for this spacecraft. The results for resonant burning were computed using the analysis approach described in Sec. V, with forcing functions defined by the Peacekeeper Q04A static firing pressure oscillation history. The Q04A test exhibited the largest pressure oscillation amplitude in the set of Peacekeeper motors used for Taurus load analyses (see Sec. IV and Table 1). Figure 5 shows that resonant burning dominates the axial response above about 50 Hz. Because coupled axial–lateral structural modes exist, it also forms the envelope of the shock spectra in the lateral directions above 50 Hz.

Passive devices that interfere with the motor acoustic modes,[20] as well as active control of some combustion parameters,[21] have been investigated for reduction of pressure oscillations from resonant burning. It does not appear that any of the existing launch vehicles have implemented these mitigation techniques. However, spacecraft isolation has been used to attenuate structural responses from resonant burning on, to date, three Taurus missions.[5]

IV. Statistical Assessments

At a given pressure oscillation frequency, the magnitude of the spacecraft loads induced by resonant burning is proportional to the

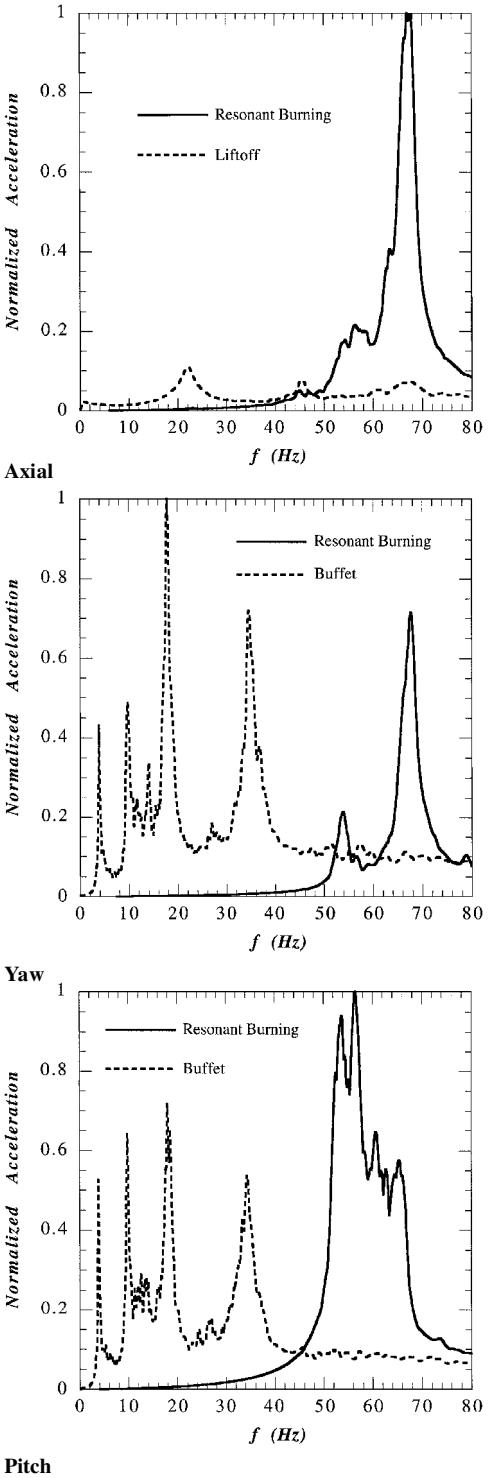

Fig. 5 Absolute shock spectra of predicted spacecraft c.g. accelerations for Taurus load events: resonant burning defines spectral envelope above approximately 50 Hz.

pressure oscillation amplitude. This amplitude changes with respect to the burning time, but, perhaps more important, the absolute maximum value varies in a set of motors. The range of this variation can be quite large, even if the physical differences between motors are reported to be negligible. Spacecraft loads from resonant burning can, therefore, vary dramatically from flight to flight.

The results of structural dynamic analyses are loads, with a specified probability of nonexceedance, used to establish the launch vehicle–space vehicle design.[19] To compute these loads, it is necessary to define an appropriate probability distribution. An incorrect choice of the distribution can cause the design loads to be significantly under- or overpredicted. Underprediction of design loads can lead to hardware failure during flight, whereas overprediction can motivate unnecessary design changes.

If there are a sufficient number of pressure oscillation histories, launch-vehicle and space-vehicle loads can be computed using a corresponding set of forcing functions. In this case, the design loads can be rigorously established after assessment, individually, of their probability distributions. Launch vehicles for which structural dynamic analyses of this type can be conducted include the space shuttle and Taurus because numerous pressure oscillation histories exist for the shuttle solid rocket booster (SRB)[12] and the Peacekeeper.[16]

Currently, static firing tests cost roughly $2 million–$50 million (or, as much as twice the cost of the test article) depending on the amount of instrumentation and the motor's size. Hence, for financial reasons, it is typical that only a few pressure oscillation histories are available after motor development for structural dynamic analyses.

In some cases, it may be reasonable to appropriate data from static firings of a similar motor design. For example, Peacekeeper data have been used for characterization of Castor 120 resonant burning.[10] Pressure oscillation histories, of course, can also be acquired during flight; this benefits post flight reconstruction efforts and load predictions for subsequent missions. However, if insufficient static firing data are available, spacecraft design for early flights in the launch vehicle manifest must account for higher uncertainty in the resonant-burning event.

Shuttle SRB[12] and Peacekeeper[16] data are investigated in this section to gain insight into the statistical characteristics of the resonant-burning phenomenon. The former is a large multisegment motor, whereas the latter is a small single-segment motor. The objective is to determine if a single probability distribution applies for resonant burning. If so, it may be reasonable to assume this distribution for solid rocket motors with an insufficient number of test or flight data samples.

A. Pressure Oscillations

In Ref. 12, space shuttle SRB pressure oscillation amplitudes were comprehensively tabulated over 5-s intervals. Table 1 lists analogous amplitudes corresponding to the Peacekeeper fundamental acoustic mode. The 50–65 Hz content of the Peacekeeper static firing histories was extracted with a six-pole Butterworth filter, and the peak-to-peak amplitudes for consecutive 3-s intervals were logged. Figure 6 shows the data tabulated for the Peacekeeper PAS02 static firing.

Plotting data points using probability scales is a simple and useful means of determining a data set's probability distribution. In this approach, the scales of the data (x axis) and cumulative probability (y axis) are modified such that the cumulative probability distribution function becomes a straight line. Because of the random character of a sample, the plotted data may not appear as a perfectly

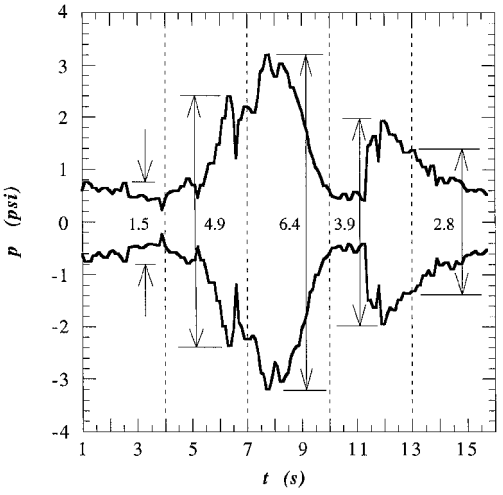

Fig. 6 Envelope of maximum and minimum values for Peacekeeper PAS02 static firing pressure oscillation history: labeled amplitudes are logged in Table 1.

straight line; however, the departures due to randomness are generally small, so that an objective decision can be made about the candidate distribution by examining the (global or regional) fit in the probability plot.

The normal, lognormal, Gumbel, and Frechet distributions were considered herein. The lognormal and normal distributions were used in Refs. 4 and 12, respectively. The Gumbel and Frechet distributions are candidates because they are distributions that occur for maxima of independent trials.[22] In other words, provided that the samples are independent, a data set of pressure oscillation amplitudes converges to the Gumbel or Frechet distribution as the number of samples becomes large.

The pressure oscillation amplitudes for the shuttle SRB and Peacekeeper were plotted for each candidate probability distribution and time interval. Figure 7 shows these plots for the Peacekeeper motor during the 4–7 s time period. The straight lines are weighted least-squares fits to the data, where the largest data values have the largest weights; this approach yields lines designed to fit primarily the right tail of the distribution.

The probability distributions that best characterize the shuttle SRB and Peacekeeper data are listed in Table 2 for each time interval. A second choice is provided when more than one probability distribution adequately models the data. Coefficient of determination values were used to establish these choices, but the plots were inspected visually for reasonableness.

The lognormal distribution is either the best fit or the second choice for all but one time segment. (The shuttle SRB data set for 95–100 s is best modeled by the Frechet distribution; however, the departures exhibited by the corresponding lognormal probability plot are not significant enough to conclude that the data did not come from a lognormal population.) It, therefore, appears that the pressure oscillation amplitudes, for both small single-segment and large multisegment motors, may generally be represented by a lognormal probability distribution. A corollary is that a lognormal distribution may be the best choice when there is insufficient static firing data to establish conclusively the probability distribution.

Table 2 Probability distribution of pressure oscillation amplitude

	Distribution(s)	
Interval, s	Best fit	Second choice
	Shuttle SRB	
0–5	Lognormal	——
5–10	Lognormal	——
10–15	Lognormal	——
15–20	Lognormal	——
20–25	Lognormal	——
25–30	Lognormal	Gumbel
30–35	Lognormal	Gumbel
35–40	Lognormal	——
40–45	Lognormal	Frechet
45–50	Lognormal	——
50–55	Lognormal	——
55–60	Lognormal	——
60–65	Lognormal	——
65–70	Lognormal	Gumbel
70–75	Lognormal	——
75–80	Lognormal	Gumbel
80–85	Normal	Lognormal
85–90	Lognormal	——
90–95	Frechet	Lognormal
95–100	Frechet	—–
100–105	Lognormal	Gumbel
105–110	Normal	Lognormal
110–115	Gumbel	Lognormal
115–120	Gumbel	Lognormal
	Peacekeeper	
1–4	Lognormal	——
4–7	Lognormal	Normal
7–10	Normal	Lognormal
10–13	Lognormal	——
13–16	Gumbel	Lognormal

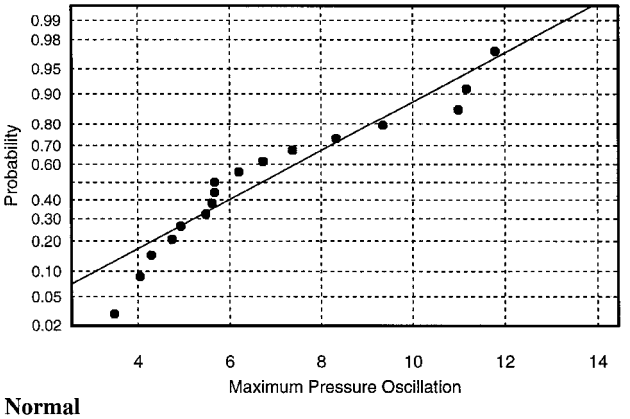

Normal

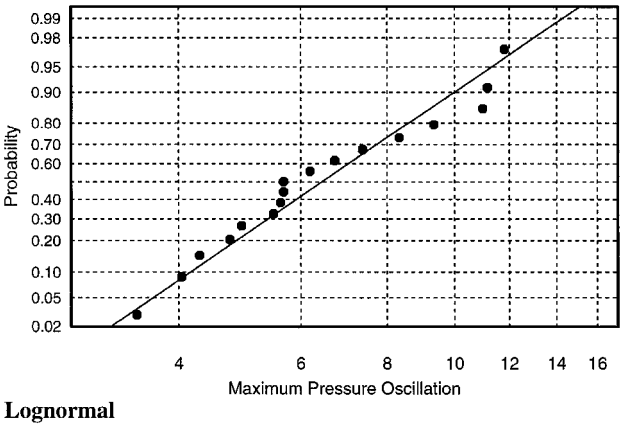

Lognormal

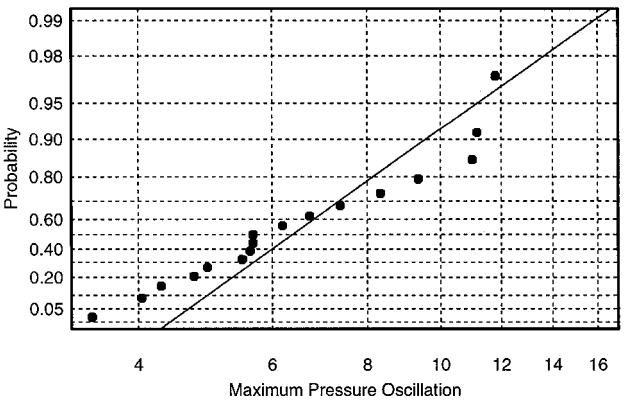

Frechet

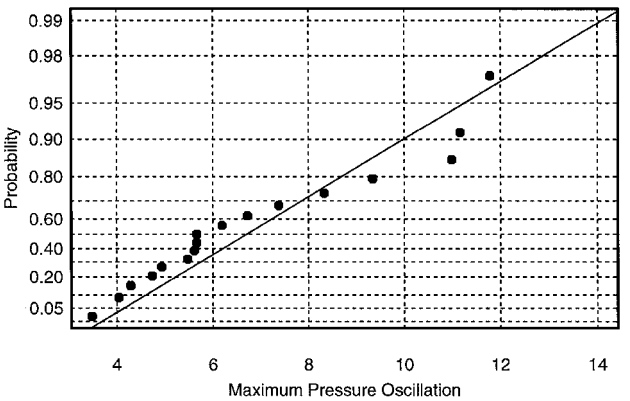

Gumbel

Fig. 7 Probability plots for Peacekeeper pressure oscillation amplitudes in 4–7 s time period: lognormal distribution yields the best fit.

The sensitivity of the enclosure value to the selection of the probability distribution is evident in Fig. 7. Based on the coefficient of determination values and visual inspection, the lognormal distribution is deemed superior to the other candidates for this example. The normal distribution is considered adequate and is a second choice. However, if the normal distribution were used a priori, a 99% enclosure value of 13.3 psi would have been reported, rather than 14.3 psi based on the lognormal distribution, an underprediction of 7%. The lognormal distribution generally yields a higher enclosure value than the normal distribution because it has a longer tail.

B. Spacecraft Loads

It follows from the preceding section that the maxima of the shuttle SRB and Peacekeeper thrust oscillations generally have a lognormal probability distribution. It does not, however, follow that the maxima of resonant-burning spacecraft loads induced during flights of the space shuttle and Taurus are also lognormal. Random vibration theory[23] shows that a simple relationship between input and output probability distributions only exists for the case in which the input is normal; in this case, the output also has a normal probability distribution.[23] The implication is that the distribution of the load maxima from resonant-burning cases must be assessed before design values can be accurately predicted and that a lognormal distribution should not be inferred.

Resonant-burning spacecraft loads were analyzed for a Taurus mission with the Peacekeeper motor as the first stage. Loads were computed at 63 payload locations using forcing functions derived from the 17 static firing tests listed in Table 1. The maximum load values at each of the 63 payload locations were tabulated for each of the 17 resonant-burning cases. Probability plots were then constructed for the normal, lognormal, Gumbel, and Frechet distributions. The best fits to the spacecraft load data are summarized in Table 3. As before, a second choice is provided when more than one probability distribution adequately models the data.

The load maxima for this Taurus mission were predominately defined by resonant burning during the 4–7 s time period. The pressure oscillation amplitude, and corresponding forcing function, have a lognormal distribution during this interval (see Fig. 7). Table 3 confirms that the spacecraft loads cannot generally be represented by a single probability distribution. However, the normal and lognormal distributions adequately model all of the results; the former characterizes about half of the loads computed for this spacecraft. Figures 8 and 9 show example plots for two of the spacecraft locations. The normal and lognormal distributions best model the data in Figs. 8 and 9, respectively.

Dynamic loads from a linear process can be defined as the sum of modal contributions. When a single term dominates this summation, the coupled dynamic model effectively reduces to a single-degree-of-freedom system, and the load has the same probability distribution as the forcing function. If, on the other hand, the summation consists of several modal responses of similar magnitude, it can be shown using the central limit theorem that the load will approach a normal distribution, regardless of the forcing function's probability distribution.[24] This explains the summary in Table 3; the spacecraft loads classified as lognormal are generally dominated by excitation of a single mode, whereas those classified as normal are composed of several modal contributions of comparable size.

Table 3 Probability distribution of spacecraft load amplitudes for a Taurus mission

Distribution		Percentage
Best fit	Second choice	of locations
Normal	——	54
Lognormal	——	19
Frechet	Lognormal	10
Lognormal	Gumbel	8
Lognormal	Frechet	6
Lognormal	Normal	1.5
Gumbel	Normal	1.5

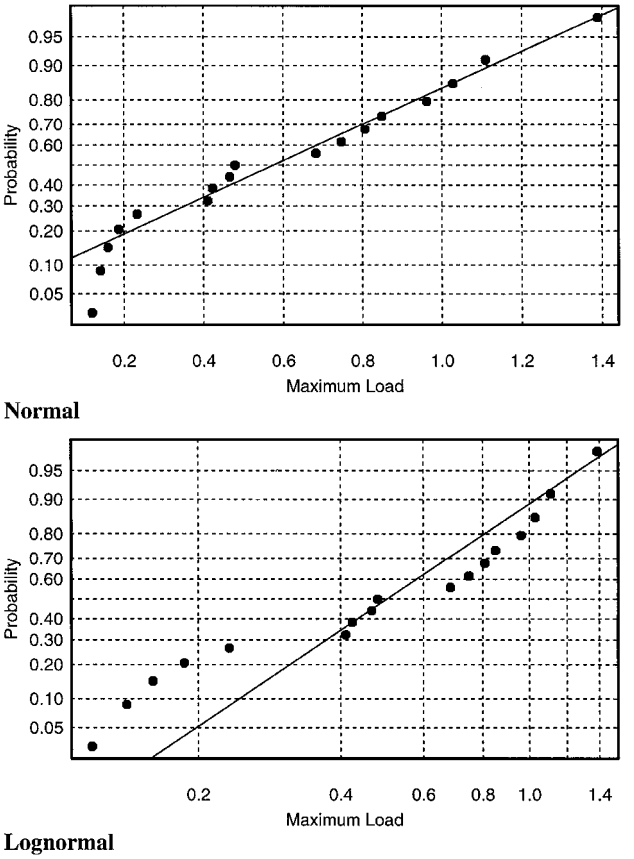

Fig. 8 Example of a spacecraft location that is best fit with the normal probability distribution.

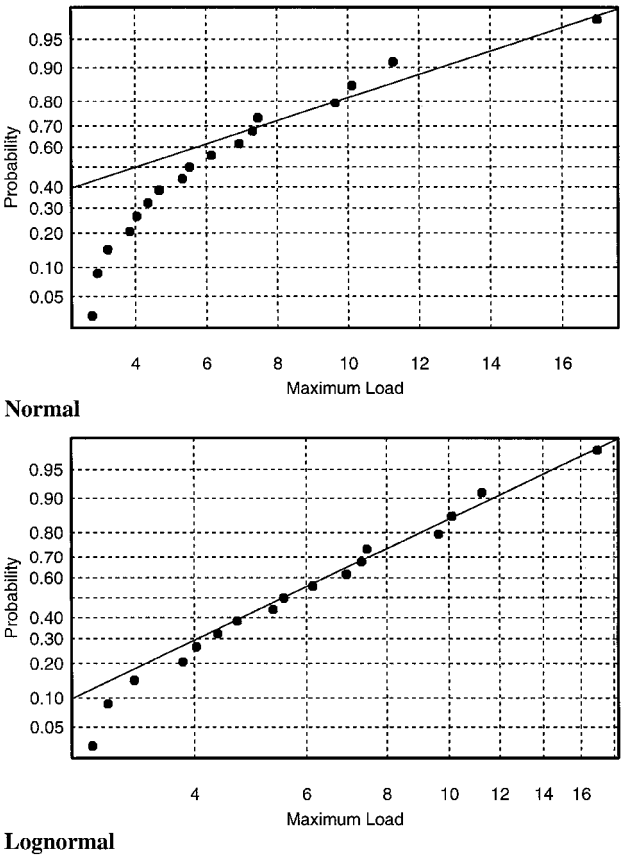

Fig. 9 Example of a spacecraft location that is best fit with the lognormal probability distribution.

It can be concluded that it is difficult to predict accurately design loads when there are too few static firing tests to construct an adequate population. Because the lognormal distribution is generally conservative with respect to the normal distribution, it may be prudent in such cases to assume that the spacecraft load maxima are lognormal, provided the response is dominated by a single mode. However, even if this distribution is adopted, the slope of the line in the probability plot must be known before design loads can be predicted. It remains to be assessed if a single slope is generally appropriate for resonant-burning load analyses.

V. Forcing Function Development

Typically, only one measurement of oscillatory pressure is taken during a test or flight, usually in the head end of the motor. This measurement may be of high fidelity depending on the characteristics of the transducer and on the quality of the data-acquisition system. Thrust can also be explicitly measured during motor tests, but generally lacks the accuracy of the pressure oscillation history because load cells register excitation of the support structure.

Accurate resonant-burning load analysis requires the force distribution internal to the solid rocket motor, which is then discretized and applied at nodes of the motor dynamic model. If the pressure oscillations are dominated by coupling with a single longitudinal acoustic mode (as it generally is), the distributed oscillatory pressure is, in a gross sense, defined by the product of the acoustic mode shape and the pressure oscillation measurement. The forcing functions for the load case, that is, static firing, equal the local pressure history times the applicable surface area.

The motor acoustic mode shape must be accurately computed for resonant-burning load analyses. The simple assumption, used in Eq. (1), that the combustion chamber is one dimensional with closed ends, is generally inadequate for forcing function development. Finite element[25] or motor-performance[26] codes can be used to predict acoustic mode shapes and frequencies. Because changes in the motor geometry affect the results, the internal surface must be established for the flight time of interest. The time period over which the acoustic mode shape can be considered constant must also be assessed before conducting the structural dynamic analysis.

A finite element (NASTRAN) model was built to calculate the longitudinal acoustic modes of the Taurus first-stage motor chamber. The Peacekeeper model included the propellant fins and webs, as well as the space between the forward dome and forward propellant face. It was established during the modeling effort that these details significantly affect the modal results. The centerline points for the calculated fundamental acoustic mode are shown in Fig. 10. The mode shape for a simple one-dimensional chamber with closed ends is included for comparison. Note that the modal amplitude at the nozzle is only 40% of the value at the forward end of the motor.

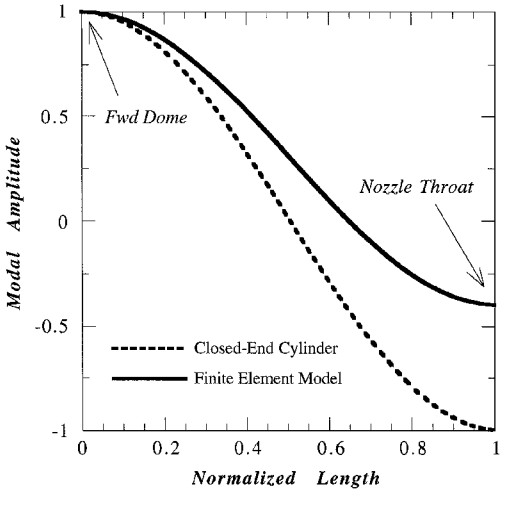

Fig. 10 Peacekeeper fundamental acoustic mode shape: closed-end cylinder approximation included for comparison.

VI. Load Analysis with a Single Resonant-Burning Case

In Sec. IV, it was shown that a lognormal probability distribution appropriately models the pressure oscillation amplitudes for both a large multisegment and a small single-segment motor. Given a probability plot with a sufficient static firing population, a design amplitude value can be readily derived. If insufficient static firing tests were conducted to form a population, and the motor is similar in design to one for which an adequate population exists, it may be acceptable to adopt a limit pressure oscillation amplitude.

With the limit amplitude defined, it may at first glance seem adequate simply to scale an existing pressure oscillation history (all motors undergo at least one static firing test) to create a worst-case forcing function for structural dynamic analyses. However, the derived forcing function may still not be conservative for all of the system structural modes because flight-to-flight frequency variations are ignored in this approach. Spectral analysis of static firing data for a variety of motors shows that frequency changes in the pressure oscillation measurements are not strictly repeatable, even if the test motors are of ostensibly identical construction. For example, Fig. 3 shows that pressure oscillations corresponding to $m = 4$ (four vortices between the propellant fins and nozzle) began at 63 Hz and persisted until 50 Hz for the PQA08 test, but were perceptible only over the range 55–58 Hz for the FP03 test. Obviously, thrust oscillations based on scaled PQA08 test data will excite a broader band of coupled launch vehicle–space vehicle structural modes, even though, from a maximum amplitude standpoint, the FP03 test represents a more severe resonant-burning case (see Table 1).

There are other features of vortex-induced pressure oscillations that make structural dynamic analysis with a single resonant-burning case difficult. Experience has shown that vortex shedding corresponding to a particular value of m may persist for so long that the subsequent jump skips an integer m value[9]; the result is a larger than normal increase in pressure oscillation frequency at the transition. The frequency tracks can also overlap during the change from one m value to the next, so that the pressure oscillations temporarily consist of two closely spaced frequencies.[9] The beating phenomenon that results may excite more coupled launch vehicle–space vehicle modes than when the frequency tracks do not overlap. These observations suggest that greater confidence can be placed in load predictions that are based on a large set of resonant-burning cases rather than on a single "worst" case. When the latter is unavoidable because of a scarcity of static firing data, application of a dynamic uncertainty factor to the computed loads may be warranted.

Given the uncertainty in the flight-to-flight frequency variation, it might appear appropriate simply to create a conservative forcing

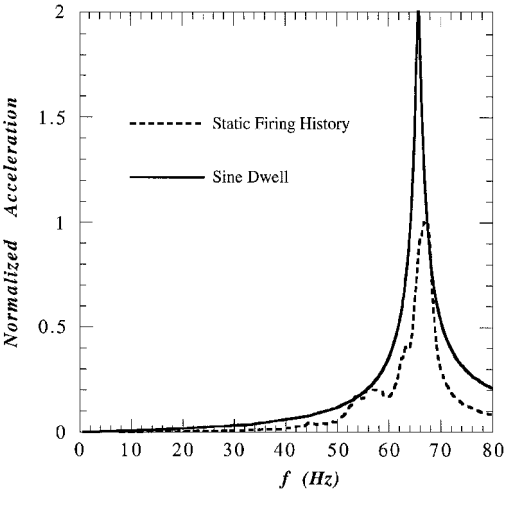

Fig. 11 Absolute shock spectra of predicted spacecraft c.g. axial acceleration for Taurus resonant-burning event: responses based on static firing data are much lower than those from sine-dwell assumption.

function that dwells at a constant frequency and amplitude. This approach implies that the vortex shedding strictly locks onto the longitudinal acoustic mode frequency and that the pressure oscillations are steady state rather than quasi periodic. Figure 11 shows an absolute shock spectrum of spacecraft c.g. axial acceleration for a Taurus mission computed using this approximation. The maximum pressure oscillation from the Peacekeeper Q04A static firing test was chosen as the sine-dwell amplitude, and the forcing function was tuned to 66 Hz, the natural frequency of the third coupled system axial mode. For this example, the spectral amplitude from the sine-dwell approach is twice as large as that computed using the nonstationary Q04A static firing history.

Conclusions

It has been shown that pressure oscillations due to resonant burning can exhibit considerable variability in amplitude and frequency, even when the test motors are of ostensibly identical construction. Although this variability does not compromise a motor's performance, it can have an important effect on structural loads induced by resonant burning. Moreover, because solid rocket motors are generally qualified based on a small number of static firing tests, the statistical enclosure for flight load nonexceedance can be difficult to compute reliably. In the past, these issues have received scant attention because solid rocket motor thrust oscillation has not been an excitation source that established design loads for medium- and heavy-lift launch vehicles. Resonant burning, however, is a critical flight event for a new class of small-sized launch vehicles with solid rocket motors as stages. For these systems, it is necessary to compute launch vehicle and space vehicle loads without introducing excessive conservatism. This renders a steady-state assumption about the phenomenon unsatisfactory and highlights the importance of acquiring suitable pressure oscillation histories from static firing tests.

More statistical studies of the type conducted in this work would help to reduce structural load uncertainty that exists when the motors used have not undergone an extensive test program. For example, the lognormal probability distribution proposed in this work for pressure oscillation amplitude should be investigated further through statistical analysis of other motors with a large static firing population. Improvements in the ability of combustion stability theory to predict pressure oscillations induced by vortex shedding would also greatly benefit structural dynamic analyses. In particular, tools are needed for the computation of pressure oscillation amplitudes induced by resonant burning.

Acknowledgment

This work was supported by the U.S. Air Force Materiel Command, Space and Missile Systems Center under Contract MDA972-89-C-0089.

References

[1]Isakowitz, S. J., *International Reference Guide to Space Launch Systems*, 2nd ed., AIAA, Washington, DC, 1995, pp. 29–47, 229–307.

[2]Culick, F. E. C., and Yang, V., "Prediction of the Stability of Unsteady Motions in Solid-Propellant Rocket Motors," *Nonsteady Burning and Combustion Stability of Solid Propellants*, edited by L. DeLuca, E. W. Price, and M. Summerfield, Vol. 143, Progress in Astronautics and Aeronautics, AIAA, Washington, DC, 1992, pp. 719–779.

[3]Kern, D. L., Himmelblau, H., Piersol, A. G., Manning, J., and Rubin, S., "Guidelines for Dynamic Environmental Criteria," NASA-HDBK-7005, Sept. 2000.

[4]Cuthbert, B., "Analysis of the LLV-1 Loads Generated by Motor Sine Vibration," Spacecraft and Launch Vehicle Dynamics Environment Technical Interchange Meeting, The Aerospace Corp., El Segundo, CA, June 1994.

[5]Wilke, P. S., Johnson, C. D., and Grosserode, P. J., "GFO/ Taurus Whole-Spacecraft Vibration Isolation System," 12th AIAA/USU Conf. on Small Satellites, A99-10826-01-20, Aug. 1998, p. 10.

[6]Price, E. W., "History of Solid Rocket Motors (1940-1960)," AIAA Paper 98-3978, July 1998.

[7]Brown, R. S., Dunlap, R., Young, S. W., and Waugh, R. C., "Vortex Shedding as a Source of Acoustic Energy in Segmented Solid Rockets," *Journal of Spacecraft and Rockets*, Vol. 18, No. 4, 1981, pp. 312–319.

[8]Kourta, A., "Vortex Shedding in Segmented Solid Rocket Motors," *Journal of Propulsion and Power*, Vol. 12, No. 2, 1996, pp. 371–376.

[9]Dotson, K. W., Koshigoe, S., and Pace, K. K., "Vortex Shedding in a Large Solid Rocket Motor Without Inhibitors at the Segment Interfaces," *Journal of Propulsion and Power*, Vol. 13, No. 2, 1997, pp. 197–206.

[10]Johnson, B. G., and Allen, A. S., "Castor 120® Motor Maximum Expected 1-L Resonant Burn Thrust Response," *Joint Army-Navy-NASA-Air Force (JANNAF) Propulsion Meeting*, CPIA Publ. 650, Vol. 1, Chemical Propulsion Information Agency, Columbia, MD, 1996, pp. 249–262.

[11]Flandro, G. A., and Jacobs, H. R., "Vortex-Generated Sound in Cavities," AIAA Paper 73-1014, Oct. 1973.

[12]Blomshield, F. S., and Bicker, C. J., "Pressure Oscillations in Shuttle Solid Rocket Motors," AIAA Paper 97-3252, July 1997.

[13]Scippa, S., Pascal, P., and Zanier, F., "Ariane 5–MPS–Chamber Pressure Oscillations Full Scale Firings Results Analysis and Further Studies," AIAA Paper 94-3068, June 1994.

[14]Nesman, T., "RSRM—Chamber Pressure Oscillations: Full Scale Ground and Flight Test Summary and Air Flow Test Results," *Proceedings of the Solid Rocket Motor Combustion Instability Workshop*, AIAA, Washington, DC, 1995, pp. 27–48.

[15]Ringgenberg, B. R., "Test Report for Static Test of Delta II Motor QM-7 (K-049)," Missiles, Ordnance, and Space Group, Bacchus Works, Subcontract 91797019, Hercules Aerospace Co., Magna, UT, May 1993.

[16]Hardy, K., "Final Report on Characterization of Peacekeeper Resonant Burn," Orbital Sciences Corp., Rept. 009-383, Chandler, AZ, Jan. 1997.

[17]Price, E. W., and Flandro, G. A., "Status and Prospects for Future Developments," *Nonsteady Burning and Combustion Stability of Solid Propellants*, edited by L. DeLuca, E. W. Price, and M. Summerfield, Vol. 143, Progress in Astronautics and Aeronautics, AIAA, Washington, DC, 1992, pp. 849–873.

[18]Mathes, H. B., "Applications of Combustion-Stability Technology to Solid-Propellant Rocket Motors," *Nonsteady Burning and Combustion Stability of Solid Propellants*, edited by L. DeLuca, E. W. Price, and M. Summerfield, Vol. 143, Progress in Astronautics and Aeronautics, AIAA, Washington, DC, 1992, pp. 781–804.

[19]Kabe, A. M., "Design and Verification of Launch and Space Vehicle Structures," AIAA Paper 98-1718, April 1998.

[20]Ramohalli, K., "Technologies and Techniques for Instability Suppression in Motors," *Nonsteady Burning and Combustion Stability of Solid Propellants*, edited by L. DeLuca, E. W. Price, and M. Summerfield, Vol. 143 Progress in Astronautics and Aeronautics, AIAA, Washington, DC, 1992, pp. 805–848.

[21]McManus, K. R., Poinsot, T., and Candel, S. M., "A Review of Active Control of Combustion Instabilities," *Progress in Energy and Combustion Science*, Vol. 19, Feb. 1993, pp. 1–29.

[22]Castillo, E., *Extreme Value Theory in Engineering*, Academic, San Diego, CA, 1988, pp. 97–101.

[23]Newland, D. E., *Random Vibrations and Spectral Analysis*, 2nd ed., Wiley, New York, 1984, pp. 79–81.

[24]Pfeiffer, P. E., and Schum, D. A., *Introduction to Applied Probability*, Academic, New York, 1973, pp. 340–342.

[25]Herting, D. N., Joseph, J. A., Kuusinen, L. R., and MacNeal, R. H., "Acoustic Analysis of Solid Rocket Motor Cavities by a Finite Element Method," NASTRAN: Users Experience, NASA TM X-2378, Sept. 1971, pp. 285–324.

[26]Nickerson, G. R., Culick, F. E. C., and Dang, A. L., "Solid Propellant Rocket Motor Performance Computer Program (SPP), Version 6.0," Air Force Astronautics Lab., Edwards Air Force Base, CA, TR-87-078, Dec. 1987.